BIOCHEMISTRY
including biophysical chemistry & molecular biology

Article

pubs.acs.org/biochemistry

Investigation of the Role of Arg301 Identified in the X-ray Structure of Phosphite Dehydrogenase

John E. Hung,[†] Emily J. Fogle,[†] Harry D. Christman,[‡] Tyler W. Johannes,[§] Huimin Zhao,[§] William W. Metcalf,[‡] and Wilfred A. van der Donk*,[†]

[†]Department of Chemistry and Howard Hughes Medical Institute, [‡]Department of Microbiology, and [§]Department of Chemical and Biomolecular Engineering, University of Illinois, 600 South Mathews Avenue, Urbana, Illinois 61801, United States

Supporting Information

ABSTRACT: Phosphite dehydrogenase (PTDH) from *Pseudomonas stutzeri* catalyzes the nicotinamide adenine dinucleotide-dependent oxidation of phosphite to phosphate. The enzyme belongs to the family of D-hydroxy acid dehydrogenases (DHDHs). A search of the protein databases uncovered many additional putative phosphite dehydrogenases. The genes encoding four diverse candidates were cloned and expressed, and the enzymes were purified and characterized. All oxidized phosphite to phosphate and had similar kinetic parameters despite a low level of pairwise sequence identity (39−72%). A recent crystal structure identified Arg301 as a residue in the active site that has not been investigated previously. Arg301 is fully conserved in the enzymes shown here to be PTDHs, but the residue is not conserved in other DHDHs. Kinetic analysis of site-directed mutants of this residue shows that it is important for efficient catalysis, with an ∼100-fold decrease in k_{cat} and an almost 700-fold increase in $K_{m,phosphite}$ for the R301A mutant. Interestingly, the R301K mutant displayed a slightly higher k_{cat} than the parent PTDH, and a more modest increase in K_m for phosphite (nearly 40-fold). Given these results, Arg301 may be involved in the binding and orientation of the phosphite substrate and/or play a catalytic role via electrostatic interactions. Three other residues in the active site region that are conserved in the PTDH orthologs but not DHDHs were identified (Trp134, Tyr139, and Ser295). The importance of these residues was also investigated by site-directed mutagenesis. All of the mutants had k_{cat} values similar to that of the wild-type enzyme, indicating these residues are not important for catalysis.

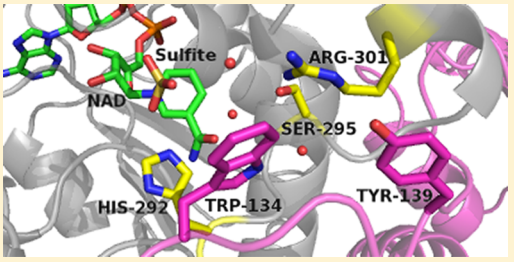

Phosphite dehydrogenase (PTDH) endows microorganisms with the ability to grow using phosphite (PT) as the sole source of phosphorus.[1] PTDH catalyzes the oxidation of phosphite to phosphate with the concurrent reduction of NAD^+ to NADH (Scheme 1). The reaction resembles a phosphoryl transfer process in which water or hydroxide acts as the phosphoryl acceptor and hydride acts as the phosphoryl donor. Thus, this reaction presents an unusual example of an enzyme catalyzing a nucleophilic displacement reaction with a hydride leaving group. Although at first glance this appears to be an unfavorable process, analysis of the thermodynamics of the reaction indicates it is 15 kcal/mol exergonic.[2] As a result, the enzyme from *Pseudomonas stutzeri* WM88 has been adapted for use in cofactor regeneration,[3] and mutants with increased activity[4] and decreased substrate specificity[5,6] have been engineered, allowing the enzyme to accept NADP as a substrate. PTDH with dual cofactor specificity has been fused to flavin monooxygenases, and the resulting self-sufficient biocatalysts have been demonstrated to have excellent activities for enantioselective catalysis.[7−9]

Scheme 1

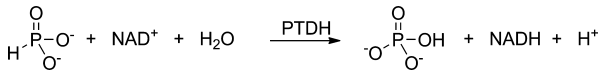

The accompanying paper (DOI 10.1021/bi2016926) describes the X-ray structure of a thermostable PTDH mutant (TS-PTDH). TS-PTDH contains 12 mutations that result in considerably increased thermostability with minimal change in activity, and four additional mutations that increase its activity[10] (for mutations, see Materials and Methods). An additional E175A mutation allows this mutant to use both NAD^+ and NADP, and this mutant that is most versatile for cofactor regeneration is termed 17X-PTDH. The X-ray structures of 17X-PTDH and TS-PTDH show very similar positions of active site residues (DOI 10.1021/bi2016926). The kinetic isotope effects, pH dependence, and pre-steady state kinetics observed with 17X-PTDH are all very similar to those observed with wild-type (wt) PTDH,[11] suggesting that these two proteins use the same mechanism of catalysis. Kinetic isotope effect (KIE) studies with deuterium-labeled phosphite and pre-steady state studies have shown that hydride transfer is fully rate-limiting.[11,12] The sequence of PTDH is ∼25−40% identical with that of the family of D-hydroxy acid

Received: November 10, 2011
Revised: May 6, 2012
Published: May 7, 2012

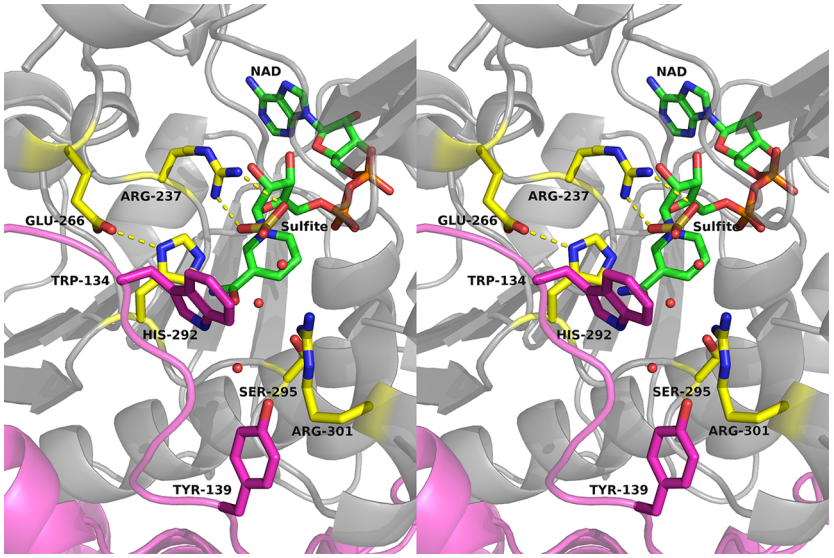

Figure 1. Stereoview of the active site of TS-PTDH containing NAD^+ and a sulfite inhibitor. His292 is the likely catalytic base; Glu266 is hydrogen bonded to His292, and Arg237 plays a role in phosphite binding.[12,13] $Trp134^B$, $Tyr139^B$, and Ser295 are hydrogen bonded to Arg301; residues colored pink are from monomer B, whereas all other residues are from monomer A. Note that the sulfite–NAD^+–PTDH complex may not be an exact representation of the active form of the ternary complex with phosphite and must be used with caution. An image presenting phosphite modeled in place of sulfite is presented in Figure S1 of the Supporting Information.

dehydrogenases (DHDHs), including several residues that have well-defined roles in these enzymes. Site-directed mutagenesis studies of these amino acids have provided some insights into the mechanism of phosphite oxidation,[12,13] but many questions remain. For instance, it is not known if the reaction takes place by a dissociative, concerted, or associative mechanism, in which hydride transfer occurs before, during, or after attack by the nucleophile, respectively. In addition, the timing of deprotonation of the water nucleophile is unresolved and could occur before, during, or after nucleophilic attack. For further discussion, see ref 14.

The cocrystal structure of TS-PTDH with NAD^+ and sulfite, a competitive inhibitor of phosphite,[1] revealed that Arg301 is within hydrogen bonding distance of a water molecule adjacent to sulfite (DOI 10.1021/bi2016926). Arg301 is not conserved among members of the DHDH family, and hence, it was not investigated in previous studies. However, as shown in this study, Arg301 is conserved in putative PTDH proteins (vide infra). Hydrogen bonded to Arg301 are two other conserved residues, Ser295 and Tyr139, and Trp134 interacts with Arg301 through a water-mediated hydrogen bonding network (Figure 1). Tyr139 and Trp134 are contributed by the second monomer in the dimeric protein.

For wt-PTDH, the pH–rate profile for $k_{cat}/K_{m,phosphite}$ shows a bell-shaped curve indicating that for optimal catalysis one group (on the protein or the substrate) must be deprotonated and another group must be protonated.[12] The pK_a values deduced from the curve are 6.8 and 7.8, respectively. The lower pK_a corresponds well to the second acid dissociation constant of phosphorous acid (the conjugate acid of phosphite), suggesting that the enzyme may utilize the dianionic form of the substrate. The higher pK_a would then correspond to an enzyme residue that must be protonated. One candidate would be His292 (Figure 1), but if so, it could not be the catalytic base that deprotonates the water nucleophile. One scenario that would still allow His292 to serve as a base involves binding of dianionic phosphite to PTDH with a protonated His292, followed by the transfer of a proton from His292 to phosphite in the ternary complex because of perturbed pK_a values in the ternary complex (Figure 2). An alternative interpretation of the

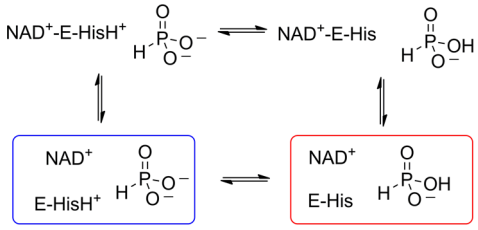

Figure 2. Possible protonation states of phosphite and His292 in PTDH. The two substrates bind to the enzyme in an ordered mechanism with NAD^+ binding first.[1] On the basis of the pH–rate profile, dianionic phosphite could bind to the NAD^+–PTDH complex containing a protonated His292 (blue). If this is the active complex, a residue other than His292 must function as a base to deprotonate the water nucleophile. Alternatively, the pK_a values of phosphite and the His could be perturbed in the ternary complex such that a proton is transferred from the protonated His to the phosphite to generate a monoprotonated phosphite as the actual electrophile (red). This form of the ternary complex could also be accessed if monoanionic phosphite binds to the NAD^+–PTDH complex in which the His is unprotonated (reverse protonation based on their pK_a values).

data is that phosphite must be protonated and His292 deprotonated for substrate binding. In this interpretation, the minor, monoprotonated form of the substrate at the optimal pH of 7.25 would bind to the minor form of the enzyme with a deprotonated His (Figure 2). Such a reverse protonation scenario would result in an identical pH–rate profile because both of these two protonation states of the substrate and enzyme would have maximal occupancy at pH 7.25, decreasing at both higher and lower pH values.[12] Because the pK_a values of the acidic and basic limbs of the PTDH pH–rate profile are separated by <2 pH units, it is difficult to differentiate between normal and reverse protonation states.[15]

dx.doi.org/10.1021/bi201691w | *Biochemistry* 2012, 51, 4254–4262

In this study, we identified putative PTDH orthologs in the protein databases and selected four members with diverse sequence identities compared to PTDH from *P. stutzeri* WM88 for heterologous expression and characterization. In addition, we used site-directed mutagenesis to investigate the importance of the Arg301, Ser295, Tyr139, and Trp134 residues.

MATERIALS AND METHODS

Materials. All chemicals were obtained from Sigma or Aldrich and used without further purification. *Methylobacterium extorquens* AM1, *Nostoc* sp. 7120, and *Ralstonia metallidurans* CH34 were obtained from ATCC. *Nostoc punctiforme* PCC 73102 was provided by J. Meeks (University of California, Davis, CA). The 16 total mutations in TS-PTDH compared to wt-PTDH from *P. stutzeri* are D13E, M26I, V71I, E130K, Q132R, Q137R, I150F, Q215L, R275Q, L276Q, I313L, V315A, A319E, A325V, E332N, and C336D. The 17X mutant has one additional mutation (E175A) that allows the protein to use both NAD^+ and NADP; it is this protein that is most versatile for cofactor regeneration. In the crystal structure of 17X-PTDH, all mutated residues are distant from the active site, with the exception of E175A, which disrupts an interaction with the ribose group of NAD^+ to allow NADP to be used as a substrate (DOI 10.1021/bi2016926).

Methods. The concentrations of NAD^+ stock solutions were determined by the absorbance at 260 nm (ε = 18000 M^{-1} cm^{-1}). The concentration of stock solutions of phosphite was determined by running the PTDH reaction to completion in the presence of excess NAD^+. The maximal absorbance at 340 nm was then measured, which represents the concentration of NADH formed (ε = 6.2 mM^{-1} cm^{-1}) and is equivalent to the concentration of phosphite consumed. Tris buffer was made from Tris base and adjusted to the correct pH with 5 M HCl; MOPS and MES buffers were made by adjusting the pH using 5 M NaOH.

Cloning of ptxD Genes from Various Organisms. The following primer sets were used to amplify DNA encoding PTDHs from whole cells of each of the following organisms: *R. metallidurans* (5′-GGCGCGCCCATATGAATCATCG-GAAAATC-3′ and 5′-GGCGCGCCGGATCCC-TATGCTGCCGCGCTGG-3′), *N. punctiforme* (5′-GGCGCGCCCATATGAAACCCAAAGTTGTAAT-3′ and 5′-GGCGCGCCGGATCCTTAACTTGGACAATTGATCG-3′), and *Nostoc* sp. PCC 7120 (5′-GGCGCGCCCATATGAAAC-CAAAGGTTGTGAT-3′ and 5′-GGCGCGCC-GGATCCTGTGTGGACAACGGCTAAAA-3′). Each primer set was designed to incorporate restriction sites (underlined above) such that *Nde*I is part of the start codon and *Bam*HI or *Bgl*II is downstream of the gene. Each PCR product was digested with *Nde*I and *Bam*HI or *Bgl*II and ligated into *Nde*I- and *Bam*HI/*Bgl*II-digested pET11a (Novagen, Inc.) to obtain the circularized plasmid. The gene from *M. extorquens* was amplified from genomic DNA using the following primers: 5′-GCCAGTTCCATATGAGAGCCAAGG-3′ and 5′-CTCA-CACTCGAGTCACGGATGTCG-3′. The primers contain *Nde*I and *Xho*I restriction sites (underlined), which were used to incorporate the gene into pET28a.

Overexpression and Purification of PTDH Orthologs. Strains of *Escherichia coli* BL21(DE3) transformed with pET11a vectors containing each *ptxD* insert were grown in LB supplemented with 100 μg/mL carbenicillin. When the OD_{600} reached 0.6, cells were induced by addition of IPTG to a final concentration of 1 mM and incubated at 25 °C for 15 h. Cells were pelleted and processed using the method described in ref 1. Extracts were loaded onto a NAD^+ affinity column using FPLC (Amersham Pharmacia Biotech). The affinity resin was generated by attaching N^6-[(6-aminohexyl)-carbamoylmethyl]-NAD to a CNBr-activated Sepharose 4 Fast Flow matrix (Amersham Pharmacia Biotech). The NAD^+ derivative (125 g) was dissolved in 5 mL of a coupling solution [0.1 M $NaHCO_3$ and 0.5 M NaCl (pH 8.3)] and then bound to 4 g of matrix following the manufacturer's coupling instructions. The cell extract slurry was added to ~15 mL of swollen NAD^+ resin and packed in an XK 16/20 column (Amersham Pharmacia Biotech) to create a final column volume of ~28 mL. Unbound protein was washed off with 10 column volumes (CV) of buffer C [20 mM MOPS buffer (pH 7.25), 10% glycerol, and 1 mM dithiothreitol]. Protein was eluted by washing with 5 CV of 5 mM NAD^+ in buffer C. Fractions with the highest purity, as determined by sodium dodecyl sulfate–polyacrylamide gel electrophoresis (SDS–PAGE) were pooled; excess NAD^+ was removed by centrifugal filtration and then concentrated to at least 2 mg/mL protein [Amicon membrane, 30000 molecular weight cutoff (Millipore)]. Protein was stored at −80 °C. Each protein ran at ~35 kDa as determined by SDS–PAGE, which is consistent with the size of each subunit in the homodimer, and was highly pure (>95%) when analyzed by SDS–PAGE. The ortholog from *M. extorquens* AM1 contained a His_6 affinity tag and was purified by the method used for mutants of 17X-PTDH, as discussed below.

Preparation of 17X-PTDH Mutant Constructs. All mutants were generated in the 17X-PTDH background using the pRW2 plasmid[10] unless noted otherwise [note that this enzyme is called 12X in ref 10 but actually contains 17 mutations (see above)]. The mutants were prepared by PCR using QuikChange mutagenesis (Agilent). The following primers were used to incorporate the mutations (along with their reverse complement strands, which are not listed): R301A, 5′-GTG CGC GCG GTG GCG CTG GAG ATT GAA C-3′; R301K, 5′-GTG CGC GCG GTG AAA CTG GAG ATT GAA C-3′; S295A, 5′-CCG CAC ATA GGG GCG GCA GTG CGC GCG-3′; Y139F, 5′-C TGG CAA CCA CGG TTC TTC GGC ACG GG-3′; W134F, 5′-GC AAG TTC CGG GGC TTC CAA CCA CGG TTC TAC-3′; W134A, 5′-GC AAG TTC CGG GGC GCG CAA CCA CGG TTC TAC-3′. The mutated codon is underlined in each case. Once the mutant genes were constructed, they were sequenced in their entirety to ensure that the desired mutation was incorporated and no other mutations were generated.

Overexpression and Purification of PTDH Mutants. To obtain mutants of 17X-PTDH, we transformed chemically competent *E. coli* BL21(DE3) cells with plasmids containing the desired gene in vector pRW2 and plated them on a LB agar plate containing 100 μg/mL ampicillin. A single colony was picked and used to inoculate an overnight culture (50 mL). The cells were harvested by centrifugation, resuspended in 1 L of LB/ampicillin, and grown at 37 °C to an OD_{600} of 0.6. IPTG was added to the culture (final concentration of 0.3 mM), which was incubated at 18 °C for 16–20 h. Cells were then pelleted by centrifugation (8000*g* for 30 min), resuspended in 20 mM Tris (pH 7.6), 0.5 M NaCl, and 10% (v/v) glycerol, and stored at −80 °C. The resuspended pellet was then thawed on ice and lysed using an Avestin Emulsiflex-C3 homogenizer (15000 psi, six passes). The insoluble lysate was removed by centrifugation (15000*g* for 30 min), and the soluble lysate was

passed through a 0.44 μm filter. The enzyme was purified via FPLC (Äkta) by immobilized metal affinity chromatography with a HisTrap HP Ni^{2+} affinity column (GE Life Sciences). The column was washed with 5 CV of buffer A, followed by a gradient to 40% buffer B over 5 CV and another gradient of 2 CV to 100% buffer B [buffer A consisted of 20 mM Tris (pH 7.6), 100 mM NaCl, 10 mM imidazole, and 10% (v/v) glycerol; buffer B consisted of 20 mM Tris (pH 7.6), 100 mM NaCl, 500 mM imidazole, and 10% (v/v) glycerol]. Fractions containing 17X-PTDH mutants were identified by an activity assay and analyzed by SDS−PAGE. The fractions that showed only PTDH by SDS−PAGE were pooled and concentrated using centrifugal filtration [Amicon membrane, 30000 molecular weight cutoff (Millipore)], followed by buffer exchange or dialysis to 20 mM MOPS (pH 7.6), 100 mM KCl, and 10% glycerol. The protein purity was >95% on the basis of FPLC analysis and SDS−PAGE analysis. Specific activities for several independent purifications of each mutant were found to be comparable, further suggesting that the enzyme was highly pure. The k_{cat} values listed in Table 2 are the average of three independently purified protein batches. The protein solution was then flash-frozen and stored at −80 °C. Protein concentrations were determined in triplicate using the calculated extinction coefficient for 17X-PTDH (28000 M^{-1} cm^{-1}).[11] For Trp134 mutants, the extinction coefficient was calculated to be 21000 M^{-1} cm^{-1} (ExPASy ProtParam tool). For comparison, protein concentrations for a stock solution of 17X-PTDH were also determined by the method of Bradford,[16] using Coomassie Plus reagent (Thermo Scientific) and bovine serum albumin (BSA) to generate a standard curve. Measurements were taken at 595 nm and compared to the standard curve to determine protein concentrations, using the calculated molar mass of 17X-PTDH. Experimental measurements were taken in triplicate in each case. Concentrations of 22.4 ± 1.3 and 22.7 ± 0.1 μM were determined by absorbance at A_{280} using the calculated extinction coefficient and the Bradford method, respectively. The concentrations determined by each method were within experimental error of one another.

Steady State Kinetic Assays. Initial rates were determined using a Cary 4000 UV−vis spectrophotometer (Varian) to monitor the rate of formation of NADH using its absorbance at 340 nm (ε = 6.2 mM^{-1} cm^{-1}). Typical reactions were performed in 100 mM MOPS (pH 7.25). For 17X-PTDH, R301K, and R301A, a full set of kinetic data was collected varying both the phosphite and NAD^+ concentrations (Figure S2 of the Supporting Information). For 17X-PTDH, substrate concentrations of 0.03, 0.05, 0.07, 0.10, 0.20, and 0.50 mM were used, with 0.0910 ± 0.0004 μM enzyme. For R301K, NAD^+ concentrations of 0.02, 0.05, 0.10, 0.20, 0.50, and 1.0 mM and phosphite concentrations of 0.50, 1.0, 2.0, 5.0, 10.0, and 20.0 mM were used, with 0.126 ± 0.001 μM enzyme. For R301A, NAD^+ concentrations of 0.1, 0.2, 0.5, 1.0, 3.0, and 6.0 mM and phosphite concentrations of 9.0, 18, 45, 90, 181, and 271 mM were used, with 4.976 ± 0.022 μM enzyme. For the other mutants, NAD^+ was held at a saturating concentration of 4 mM (>16$K_{m,NAD}$) while the phosphite concentration was varied, or NAD^+ concentrations were varied while phosphite was held at a saturating concentration of 2.2 mM for S295A (21$K_{m,PT}$), 9.0 mM for W134F (26$K_{m,PT}$), 46.5 mM for W134A (24$K_{m,PT}$), and 5.0 mM for Y139F (128$K_{m,PT}$). Enzyme concentrations were 0.259 ± 0.001 μM for S295A, 0.147 ± 0.001 μM for Y139F, 0.233 ± 0.001 μM for W134A, and 0.215 ± 0.001 μM for W134F. Errors in k_{cat} were obtained from three independently purified batches of protein.

For the kinetic assays, reaction mixtures were allowed to equilibrate at 25 °C in a controlled temperature block, which was verified using a thermocouple inserted into the cuvette, and the reaction was initiated by addition of enzyme. Assays on the 17X-PTDH mutants were performed with the His_6 affinity tag attached. The His tag has been shown not to have a significant effect on the kinetic parameters of the enzyme in a previous study.[5] Assays for PTDH orthologs were performed at 30 °C. Initial rates were obtained over the course of 1 min. The data were fit to the Michaelis−Menten equation using OriginPro 8 (OriginLab) for the orthologs and the mutants of Ser295, Trp134, and Tyr139 or using the equation for an ordered, sequential, two-substrate mechanism (eq 1)[17] using GraFit 7[18] for 17X-PTDH, R301A, and R301K.

$$v = \frac{V_{max}[A][B]}{K_{ia}K_B + K_B[A] + K_A[B] + [A][B]} \quad (1)$$

In this equation A represents the first substrate to bind (NAD^+) and B represents the second substrate (phosphite). K_A and K_B are $K_{m,NAD}$ and $K_{m,PT}$, respectively. K_{ia} represents the dissociation constant for NAD^+.

Kinetic Isotope Effects. Deuterium-labeled phosphite (D-PT) was prepared as reported previously[12] by mixing phosphorous acid with deuterium oxide at 50 °C for 6 h. The solution was then concentrated with a rotary evaporator and the residue redissolved in deuterium oxide. This procedure was repeated until only deuterium-labeled phosphorous acid was observed by ^{31}P NMR spectroscopy (500 MHz Varian, H_3PO_4 used as an external reference, δ = 0 ppm): δ 3.71 (t, J_{P-D} = 88 Hz). The solution was then neutralized using aqueous NaOH and lyophilized to obtain solid deuterium-labeled sodium phosphite. We determined kinetic isotope effects (KIEs) by holding NAD^+ at saturating conditions (>10K_m) and obtaining initial rates with varying concentrations of either deuterated or protiated phosphite.

pH−Rate Profiles of 17X-PTDH Mutants. Solutions containing 100 mM Tris, 50 mM MES, and 50 mM acetic acid, generating a universal buffer with a constant ionic strength,[19] were prepared at pH 5.5, 5.8, 6.1, 6.4, 6.7, 7.0, 7.3, 7.6, 7.9, 8.2, 8.5, 8.8, and 9.0. NAD^+ was dissolved in a buffer with the desired pH, and phosphite stock solutions were adjusted to the pH of the assay. Experiments were also performed in 100 mM Tris-maleate, a broad range buffer, as well as in 100 mM MOPS from pH 6.7 to 7.7. NAD^+ was held at saturating conditions (>10K_m), whereas phosphite concentrations were varied from 0.05 to 1500 mM (for 17X-PTDH-R301A), from 0.5 to 500 mM (for 17X-PTDH-R301K), and from 0.15 to 50 mM (for 17X-PTDH). The concentrations of phosphite used at each pH were varied according to the $K_{m,PT}$ at that pH, ranging from approximately 0.2K_m to >10$K_{m,PT}$. The samples were mixed and allowed to equilibrate for several minutes to adjust the temperature and ensure homogeneity until the baseline absorbance at 340 nm remained constant. Reactions were initiated by addition of 17X-PTDH (final concentration of 0.16 μM), 17X-PTDH-R301K (final concentration of 0.08 μM), or 17X-PTDH-R301A (final concentration of 3−6 μM). Initial rates of NADH formation were monitored at 340 nm using a Cary 4000 spectrophotometer. Kinetic parameters were determined from fits to the Michaelis−Menten equation using OriginPro 8, and pK_a values were

dx.doi.org/10.1021/bi201691w | *Biochemistry* 2012, 51, 4254−4262

Table 1. Kinetic Characterization of PTDH Orthologs at 30 °C[a]

	P. stutzeri	*R. metallidurans*	*Nostoc* sp. 7120	*N. punctiforme*	*M. extorquens*
$K_{m,NAD}$ (μM)	52.2 (3.3)	4.5 (0.9)	10.3 (1.4)	19.4 (1.6)	40.5 (11.1)
$K_{m,PT}$ (μM)	81.1 (1.6)	54.9 (6.8)	20.2 (1.6)	25.4 (1.2)	237 (36)
k_{cat} (s^{-1})	6.57 (0.03)	6.83 (0.43)	2.41 (0.03)	3.36 (0.03)	5.10 (0.14)

[a]Errors in parentheses were obtained from fits to the Michaelis–Menten equation. Errors in k_{cat} do not include any errors in protein concentration. The enzyme from *M. extorquens* contained an N-terminal His_6 tag, whereas the other enzymes did not.

Table 2. Steady State Parameters of 17X-PTDH Mutants[a]

	k_{cat} (s^{-1})	$K_{m,PT}$ (mM)	$K_{m,NAD}$ (mM)	$K_{ia,NAD}$ (mM)	$k_{cat}/K_{m,PT}$ (M^{-1} s^{-1})	$^{D}k_{cat}$	$^{D}(k_{cat}/K_{m,PT})$
17X-PTDH[b]	3.27 (0.24)	0.028 (0.007)	0.022 (0.006)	1.03 (0.27)	1.17 (0.30) × 10^5	2.30 (0.04)	2.08 (0.16)
R301K[b]	4.50 (0.72)	1.11 (0.12)	0.074 (0.007)	0.97 (0.14)	4050 (780)	1.90 (0.09)	2.19 (0.49)
R301A[b]	0.041 (0.007)	19.4 (1.22)	0.216 (0.015)	0.48 (0.07)	2.11 (0.38)	2.7 (0.1)	2.1 (0.2)
S295A[c]	2.53 (0.22)	0.103 (0.017)	0.250 (0.030)	nd[d]	2.46 (0.46) × 10^4	nd[d]	nd[d]
W134F[c]	2.96 (0.10)	0.238 (0.011)	0.102 (0.006)	nd[d]	1.24 (0.07) × 10^4	2.22 (0.04)	2.68 (0.19)
W134A[c]	1.73 (0.14)	1.91 (0.11)	0.187 (0.019)	nd[d]	901 (89)	2.16 (0.05)	2.09 (0.20)
Y139F[c]	3.68 (0.37)	0.039 (0.002)	0.036 (0.002)	nd[d]	9.44 (1.07) × 10^4	nd[d]	nd[d]

[a]All assays were performed at 25 °C and pH 7.25 in 100 mM MOPS. k_{cat} values were obtained for three batches of each enzyme, and the average is presented here (see Materials and Methods). [b]We determined the values by varying the concentrations of both substrates, determining the initial rates, and fitting all data to the equation shown in Materials and Methods. [c]We determined the values by holding one substrate at a saturating concentration and varying the concentration of the other substrate. Initial rates were fit to the Michaelis–Menten equation. The errors given in parentheses were obtained from the fits of the experimental data to the respective equations (see Materials and Methods). [d]Not determined.

determined by fitting logarithmic plots of k_{cat} and k_{cat}/K_m to the equation for curves with one or two proton transitions (eqs 2 and 3, respectively),[20] with K_1, K_2, and $(k_{cat}/K_m)_0$ representing dependent variables that are calculated by fitting of the data. K_1 represents the acid dissociation constant for a proton transition that increases activity upon deprotonation (ascending limb), and K_2 represents the acid dissociation constant for a proton transition that decreases activity upon deprotonation (descending limb); $(k_{cat}/K)_0$ is a pH-independent value.

$$\log\left(\frac{k_{cat}}{K_m}\right) = \log\left[\frac{\left(\frac{k_{cat}}{K_m}\right)_0}{1 + \frac{[H^+]}{K_1}}\right] \quad (2)$$

$$\log\left(\frac{k_{cat}}{K_m}\right) = \log\left[\frac{\left(\frac{k_{cat}}{K_m}\right)_0}{1 + \frac{[H^+]}{K_1} + \frac{K_2}{[H^+]}}\right] \quad (3)$$

Gel Filtration Experiments. Gel filtration experiments were performed on a BioSil SEC-250 (Bio-Rad) HPLC gel filtration column using a buffer that consisted of 100 mM MOPS (pH 7.3) and 0.4 M sodium phosphite. Albumin, alcohol dehydrogenase, β-amylase, blue dextran, carbonic anhydrase, and cytochrome *c* standards (Sigma-Aldrich) were used to generate a standard curve. 17X-PTDH-R301A and 17X-PTDH were run on the column with and without 5 mM NAD^+. The elution time compared to that of the standards was used to determine the oligomerization states of the proteins.

RESULTS

Identification of PTDH Orthologs. Several uncharacterized proteins from different bacteria were selected to test for PTDH activity based on their level of sequence identity (44–56%) to wt-PTDH from *P. stutzeri* (Table S1 of the Supporting Information). These proteins were heterologously expressed in *E. coli*, purified by NAD^+ affinity chromatography, and assayed for PTDH activity with phosphite and NAD^+ (Table 1). NADH formation was observed spectrophotometrically, and phosphate production was verified with a malachite green assay.[21] The kinetic parameters of each protein were comparable to those of PTDH from *P. stutzeri*.

Sequence Analysis of PTDH Orthologs. Residues Arg237, Glu266, and His292 are highly conserved among the DHDH family and have been shown to be important for catalysis in PTDH.[12,13] With more than one PTDH now identified experimentally, a sequence alignment was performed to determine if any other residues are conserved among this enzyme family. On the basis of this alignment, Arg301, Ser295, Tyr139, and Trp134 were found to be highly conserved among these enzymes but not among members of the DHDH family (Figure S3 of the Supporting Information). Furthermore, all four residues are near the phosphite binding site (Figure 1). Several other conserved residues were observed, but in the crystal structure of PTDH, these residues are distant from the enzyme active site. To investigate the importance of Arg301, Ser295, Tyr139, and Trp134 for catalysis, we performed site-directed mutagenesis to generate the following mutants, all in the 17X-PTDH background: Arg301Lys, Arg301Ala, Ser295Ala, Tyr139Phe, Trp134Phe, and Trp134Ala. All mutants were successfully expressed in *E. coli* as N-terminally His_6-tagged fusion proteins and purified by immobilized Ni^{2+} affinity chromatography.

PTDH Steady State Assays. Steady state kinetic assays were used to determine the effect of each mutation on enzyme activity (Table 2). Overall, the values of k_{cat} for all mutants except Arg301Ala are very similar to that of the parent PTDH. The k_{cat} of the Arg301Ala mutant was reduced ~100-fold, but the k_{cat} of the Arg301Lys mutant was actually slightly increased compared to that of 17X-PTDH. $K_{m,PT}$ was greatly increased for both Arg301 mutants, with a particularly large increase (~700-fold) for Arg301Ala. $K_{m,NAD}$ was also increased 10-fold for the R301A mutant, with a more modest increase (3-fold) for R301K. Use of a full matrix of varying phosphite and NAD^+ concentrations allowed determination of the dissociation

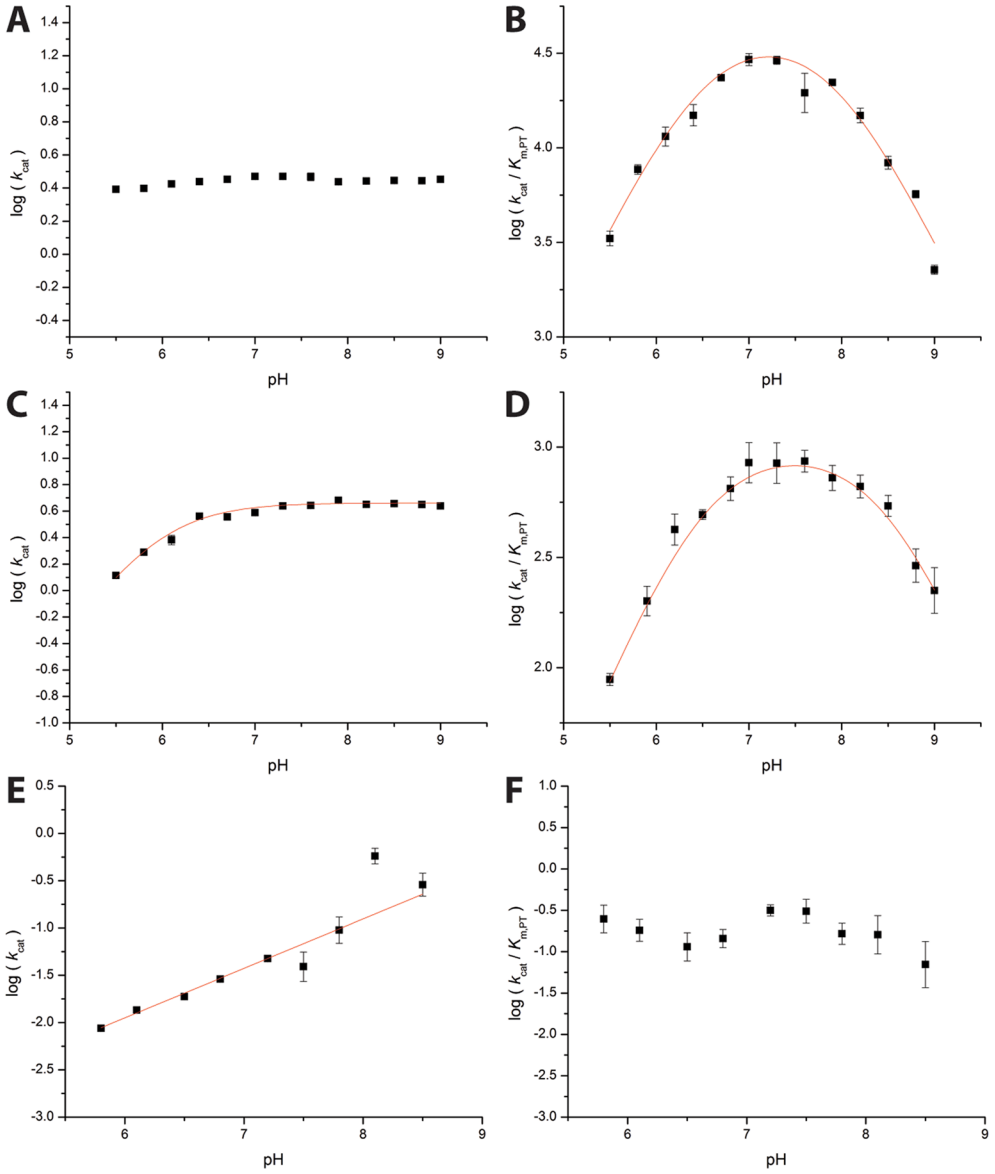

Figure 3. pH−rate profiles of log(k_{cat}) and log($k_{cat}/K_{m,PT}$) for 17X-PTDH (A and B, respectively), 17X-PTDH-R301K (C and D, respectively), and 17X-PTDH-R301A (E and F, respectively). When error bars are not visible, they were smaller than the font size used for the data point.

constant for NAD, $K_{ia,NAD}$, using the equation[22] for an ordered, sequential mechanism in which NAD^+ binds prior to phosphite.[1] Arg301 mutations did not substantially increase $K_{ia,NAD}$ (Table 2), which is perhaps not unexpected given the large distance between Arg301 and the cofactor in the crystal structure (DOI 10.1021/bi2016926). In the X-ray structure, Arg301 participates in the dimer interface for 17X-PTDH. To ensure that the data obtained with the Arg301Ala mutant were not a consequence of disruption of the oligomerization state of the protein, gel filtration experiments were performed, which showed that the Arg301Ala mutant remains a dimer.

The Ser295Ala, Trp134Phe, Trp134Ala, and Tyr139Phe mutants had only slightly reduced k_{cat} values compared to that of 17X-PTDH, suggesting that these residues do not play an important role in catalysis. Trp134 mutations did affect the K_m values for phosphite, with the Trp134Ala mutant exhibiting a 40-fold increase in $K_{m,PT}$. The Trp134Phe mutant had a similar effect on $K_{m,PT}$, although it was smaller in magnitude. Kinetic isotope effect (KIE) experiments performed with selected mutants yielded normal $^Dk_{cat}$ and $^Dk_{cat}/K_{m,PT}$ values, which were similar in magnitude to those observed with 17X-PTDH. These results suggest that hydride transfer remains rate-limiting at pH 7.25, as has been previously shown for wt-PTDH and a series of mutants with a wide range of catalytic activities.[11]

pH−Rate Profiles of 17X-PTDH Mutants. The pH dependence of the steady state kinetic constants was determined for 17X-PTDH-R301A and 17X-PTDH-R301K, the mutants with the most interesting phenotypes. Like that of wt-PTDH, the pH−rate profile for 17X-PTDH is pH-independent for log(k_{cat}) (Figure 3A) and displays a bell-shaped curve for log(k_{cat}/K_m) (Figure 3B) with extracted pK_a values of 6.53 ± 0.10 and 7.90 ± 0.08 from a fit to the appropriate equation (see Materials and Methods). The pH−rate profile for R301K was overall similar to that of 17X-PTDH. The log(k_{cat}) profile is pH-independent in the pH range of 7−9, but it appears that a deprotonation event with a pK_a of 5.93 ± 0.03 may affect k_{cat}. This pK_a is close to the limits of the pH range in which this mutant is stable (Figure 3C), and we cannot

dx.doi.org/10.1021/bi201691w | *Biochemistry* 2012, 51, 4254−4262

completely rule out the possibility that the observed decrease in activity may be the result of a loss of activity that is not associated with a defined ionizable residue. The mutant displays a bell-shaped curve for $\log(k_{cat}/K_m)$, with extracted pK_a values of 6.62 ± 0.05 and 8.37 ± 0.07 for the two proton transitions (Figure 3D).

In contrast to the plots of k_{cat}/K_m and k_{cat} of R301K, the pH dependence of the kinetic parameters of R301A was very different. The plot of $\log(k_{cat})$ versus pH was nearly linear with a slope of 0.6 (Figure 3E) and may suggest specific base catalysis by hydroxide (for further discussion, see the Supporting Information). In contrast, $\log(k_{cat}/K_m)$ was essentially pH-independent (Figure 3F). This latter finding is the result of offsetting effects on k_{cat} and $K_{m,PT}$ (Table S3 of the Supporting Information). The former increases with pH, resulting in improved catalysis, but the latter also increases with pH, resulting in less efficient catalysis at low substrate concentrations. The same findings were obtained in three different buffer systems: a universal buffer with a constant ionic strength,[19] a broad-range Tris-maleate buffer, and MOPS, the standard PTDH assay buffer. The data in Figure 3 were obtained in the universal buffer.

■ DISCUSSION

The rapid increase in the number of available protein sequences suggests that a substantial branch of the DHDH family is likely composed of phosphite dehydrogenases (Figure S4 of the Supporting Information). Four of these enzymes were shown here to catalyze phosphite oxidation to complement the previously characterized enzymes from *P. stutzeri*[1] and *Alcaligenes faecalis*.[23] Another phosphite dehydrogenase from *Pseudomonas* sp. K was reported while this paper was under review.[24] Analysis of the kinetic parameters of these enzymes illustrates that they all have similar k_{cat} values despite a high degree of sequence diversity (39−72% pairwise identity). The reaction catalyzed by PTDHs has a very strong thermodynamic driving force, and it has been suggested that perhaps the rather moderate values of k_{cat} were the result of a "young" enzyme that had relatively recently evolved from a progenitor in the DHDH family.[12] The strong sequence diversity demonstrated here suggests that instead phosphite oxidation is likely an old activity, and the very similar catalytic parameters, combined with the inability to increase k_{cat} substantially by directed evolution,[4] suggest that the rates of oxidation of phosphite by PTDHs may be limited by a relatively high intrinsic barrier.

With the recently determined crystal structure of TS-PTDH (DOI 10.1021/bi2016926) and the availability of sequences of additional PTDH orthologs with moderate sequence homology to the enzyme from *P. stutzeri*, several previously unidentified conserved residues near the active site were revealed. These amino acids include Ser295, Tyr139, Trp134, and Arg301, none of which are conserved in the DHDH family. Our mutagenesis studies do not support important roles for Ser295, Tyr139, and Trp134 in catalysis because relatively conservative mutations at these positions that removed functional groups (S295A, Y139F, and W134F) did not much alter k_{cat}. The conservative mutants of Trp134 and Ser295 did result in an increase in the K_m values of the substrates (4−10-fold), suggesting that these residues do play roles in optimizing catalytic efficiency, perhaps by helping position Arg301 to which they are hydrogen bonded in the wt enzyme.

The phenotypes of the mutants of Arg301 were more interesting. In the X-ray structure of the ternary complex with the competitive inhibitor sulfite (DOI 10.1021/bi2016926), Arg301 is hydrogen bonded to a water molecule that in turn is hydrogen bonded to sulfite. Its side chain is in a position within the PTDH active site that could be interpreted as Arg301 potentially acting as a catalytic base to deprotonate a water nucleophile. Arginine is not commonly considered in the acid−base chemistry of proteins because of its relatively high solution phase pK_a, but several recent reports have documented enzymes in which arginine has been proposed to act as a base.[25−34] The Arg301Ala mutation of 17X-PTDH resulted in an approximately 100-fold reduced k_{cat} and a greatly increased $K_{m,PT}$, demonstrating that Arg301 indeed plays an important catalytic role. The magnitude of the reduction in the k_{cat} of the Arg301Ala mutant and the observation that the Arg301Lys mutant retained a k_{cat} comparable to that of 17X-PTDH are similar to the findings with mutants of inosine monophosphate dehydrogenase for which a role of an Arg as active site base to deprotonate a water molecule has been proposed.[25−27,35,36] However, the observed phenotype of the Arg301Ala mutant may also be attributed to removal of an important electrostatic effect. Indeed, the large changes in the K_m values for both substrates as well as the drastically different pH dependence of both k_{cat} and $k_{cat}/K_{m,PT}$ suggest that this mutant is severely disrupted compared to the parent protein and that its mechanism of catalysis may not be representative of the parent enzyme. Because we have no direct experimental evidence that Arg is acting as a base, we prefer a model of Arg301 providing electrostatic activation for the nucleophilic attack of water/hydroxide on phosphite.

An electrostatic role of Arg301 appears to be supported by the data obtained for 17X-PTDH-R301K. This mutant shows a more modest increase in $K_{m,PT}$ and has a slightly improved k_{cat} compared to those of 17X-PTDH. Furthermore, the pH−rate profiles are very similar, the only substantial change being a shift of the basic pK_a in the bell-shaped curve for $\log(k_{cat}/K_{m,PT})$ to a higher value (from 7.9 to 8.4). If this pK_a indeed represents His292, its pK_a could be increased because of a weaker electrostatic destabilization of the imidazolium group of His292 by a protonated Lys than by a protonated Arg. Collectively, the steady state kinetic parameters and the pH−rate profiles suggest that lysine is capable of playing a catalytic role similar to that of arginine, and these observations are more readily explained by an electrostatic interaction than by a role as a base. These positively charged residues may also be important for orienting the phosphite substrate for efficient catalysis.

In summary, the simplest explanation of the data in this and previous studies is that His292 is associated with the basic limb and phosphite with the acidic limb of the pH−rate profile for $k_{cat}/K_{m,PT}$. Whether His292 is unprotonated and phosphite monoprotonated in the binding step, or whether dianionic phosphite binds to PTDH with a protonated His292 is currently not known, but either possibility suggests that the nucleophilic displacement reaction takes place on monoprotonated phosphite. The fully conserved Arg301 that is near the phosphite binding site in the X-ray structure appears to play an electrostatic role in catalysis given the very minor perturbations observed in the R301K mutant.

■ ASSOCIATED CONTENT

Supporting Information

Supporting figures showing a model of phosphite in the active site of PTDH, pairwise sequence identities of PTDH enzymes, steady state kinetic data, sequence alignments, and pH−rate

data. This material is available free of charge via the Internet at http://pubs.acs.org.

AUTHOR INFORMATION

Corresponding Author

*Phone: (217) 244-5360. Fax: (217) 244-8068. E-mail: vddonk@illinois.edu.

Funding

This work was supported by the National Science Foundation (Grant 0822536 to W.A.v.d.D.) and the Biotechnology Research and Development Consortium (Project 2-4-121 to W.W.M. and H.Z.).

Notes

The authors declare no competing financial interest.

ACKNOWLEDGMENTS

We appreciate the suggestion of an anonymous reviewer that proton transfer in the ternary complex provides an alternative to a reverse protonation mechanism.

ABBREVIATIONS

PTDH, phosphite dehydrogenase; *ptxD*, phosphite dehydrogenase-encoding gene; KIE, kinetic isotope effect; NAD^+, nicotinamide adenine dinucleotide; DHDH, D-hydroxy acid dehydrogenase; H-PT, phosphite; D-PT, deuterated phosphite; TS-PTDH, thermostable PTDH mutant; 17X-PTDH, TS-PTDH with the E175A mutation; CV, column volume; IPTG, isopropyl β-D-thiogalactopyranoside; PCR, polymerase chain reaction; wt, wild-type; BSA, bovine serum albumin.

REFERENCES

(1) Costas, A. M., White, A. K., and Metcalf, W. W. (2001) Purification and characterization of a novel phosphorus-oxidizing enzyme from *Pseudomonas stutzeri* WM88. *J. Biol. Chem. 276*, 17429−17436.

(2) Vrtis, J. M., White, A., Metcalf, W. W., and van der Donk, W. A. (2001) Phosphite dehydrogenase: An unusual phosphoryl transfer reaction. *J. Am. Chem. Soc. 123*, 2672−2673.

(3) Vrtis, J. M., White, A., Metcalf, W. W., and van der Donk, W. A. (2002) Phosphite Dehydrogenase, a New Versatile Cofactor Regeneration Enzyme. *Angew. Chem., Int. Ed. 41*, 3257−3259.

(4) Woodyer, R., van der Donk, W. A., and Zhao, H. (2006) Optimizing a biocatalyst for improved NAD(P)H regeneration: Directed evolution of phosphite dehydrogenase. *Comb. Chem. High Throughput Screening 9*, 237−245.

(5) Woodyer, R., van der Donk, W. A., and Zhao, H. (2003) Relaxing the nicotinamide cofactor specificity of phosphite dehydrogenase by rational design. *Biochemistry 42*, 11604−11614.

(6) Johannes, T. W., Woodyer, R., and Zhao, H. (2007) Efficient regeneration of NADPH using an engineered phosphite dehydrogenase. *Biotechnol. Bioeng. 96*, 18−26.

(7) Torres Pazmino, D. E., Snajdrova, R., Baas, B. J., Ghobrial, M., Mihovilovic, M. D., and Fraaije, M. W. (2008) Self-sufficient Baeyer-Villiger monooxygenases: Effective coenzyme regeneration for biooxygenation by fusion engineering. *Angew. Chem., Int. Ed. 47*, 2275−2278.

(8) Rioz-Martinez, A., Kopacz, M., de Gonzalo, G., Torres Pazmino, D. E., Gotor, V., and Fraaije, M. W. (2011) Exploring the biocatalytic scope of a bacterial flavin-containing monooxygenase. *Org. Biomol. Chem. 9*, 1337−1341.

(9) Torres Pazmino, D. E., Riebel, A., de Lange, J., Rudroff, F., Mihovilovic, M. D., and Fraaije, M. W. (2009) Efficient biooxidations catalyzed by a new generation of self-sufficient Baeyer-Villiger monooxygenases. *ChemBioChem 10*, 2595−2598.

(10) Johannes, T. W., Woodyer, R. W., and Zhao, H. (2005) Directed evolution of a thermostable phosphite dehydrogenase for NAD(P)H regeneration. *Appl. Environ. Microbiol. 71*, 5728−5734.

(11) Fogle, E. J., and van der Donk, W. A. (2007) Pre-steady-state studies of phosphite dehydrogenase demonstrate that hydride transfer is fully rate limiting. *Biochemistry 46*, 13101−13108.

(12) Relyea, H. A., Vrtis, J. M., Woodyer, R., Rimkus, S. A., and van der Donk, W. A. (2005) Inhibition and pH dependence of phosphite dehydrogenase. *Biochemistry 44*, 6640−6649.

(13) Woodyer, R., Wheatley, J., Relyea, H., Rimkus, S., and van der Donk, W. A. (2005) Site-directed mutagenesis of active site residues of phosphite dehydrogenase. *Biochemistry 44*, 4765−4774.

(14) Relyea, H. A., and van der Donk, W. A. (2005) Mechanism and applications of phosphite dehydrogenase. *Bioorg. Chem. 33*, 171−189.

(15) Cleland, W. W. (1977) Determining the chemical mechanisms of enzyme-catalyzed reactions by kinetic studies. *Adv. Enzymol. 45*, 273−387.

(16) Bradford, M. M. (1976) A rapid and sensitive method for the quantitation of microgram quantities of protein utilizing the principle of protein-dye binding. *Anal. Biochem. 72*, 248−254.

(17) Cleland, W. W. (1979) Statistical Analysis of Enzyme Kinetic Data. *Methods Enzymol. 63*, 103−138.

(18) Leatherbarrow, R. J. (2009) *GraFit*, version 7.0, Erithacus Software Ltd., Horley, U.K.

(19) Ellis, K. J., and Morrison, J. F. (1982) Buffers of constant ionic strength for studying pH-dependent processes. *Methods Enzymol. 87*, 405−426.

(20) Cleland, W. W. (1982) The use of pH studies to determine chemical mechanisms of enzyme-catalyzed reactions. *Methods Enzymol. 87*, 390−405.

(21) Lanzetta, P. A., Alvarez, L. J., Reinach, P. S., and Candia, O. A. (1979) An improved assay for nanomole amounts of inorganic phosphate. *Anal. Biochem. 100*, 95−97.

(22) Cook, P. F., and Cleland, W. W. (2007) *Enzyme Kinetics and Mechanism*, Garland Science, New York.

(23) Wilson, M. M., and Metcalf, W. W. (2005) Genetic diversity and horizontal transfer of genes involved in oxidation of reduced phosphorus compounds by *Alcaligenes faecalis* WM2072. *Appl. Environ. Microbiol. 71*, 290−296.

(24) Liu, D.-F., Ding, H.-T., Du, Y.-Q., Zhao, Y.-H., and Jia, X.-M. (2012) Cloning, Expression, and Characterization of a Wide-pH-Range Stable Phosphite Dehydrogenase from *Pseudomonas* sp. K in *Escherichia coli*. *Appl. Biochem. Biotechnol. 166*, 1301−1313.

(25) Guillén Schlippe, Y. V., and Hedstrom, L. (2005) Is Arg418 the catalytic base required for the hydrolysis step of the IMP dehydrogenase reaction? *Biochemistry 44*, 11700−11707.

(26) Guillén Schlippe, Y. V., and Hedstrom, L. (2005) A twisted base? The role of arginine in enzyme-catalyzed proton abstractions. *Arch. Biochem. Biophys. 433*, 266−278.

(27) Hedstrom, L., and Gan, L. (2006) IMP dehydrogenase: Structural schizophrenia and an unusual base. *Curr. Opin. Chem. Biol. 10*, 520−525.

(28) Bossi, R. T., Negri, A., Tedeschi, G., and Mattevi, A. (2002) Structure of FAD-bound L-aspartate oxidase: Insight into substrate specificity and catalysis. *Biochemistry 41*, 3018−3024.

(29) Tedeschi, G., Ronchi, S., Simonic, T., Treu, C., Mattevi, A., and Negri, A. (2001) Probing the active site of L-aspartate oxidase by site-directed mutagenesis: Role of basic residues in fumarate reduction. *Biochemistry 40*, 4738−4744.

(30) Charnock, S. J., Brown, I. E., Turkenburg, J. P., Black, G. W., and Davies, G. J. (2002) Convergent evolution sheds light on the anti-β-elimination mechanism common to family 1 and 10 polysaccharide lyases. *Proc. Natl. Acad. Sci. U.S.A. 99*, 12067−12072.

(31) Mowat, C. G., Moysey, R., Miles, C. S., Leys, D., Doherty, M. K., Taylor, P., Walkinshaw, M. D., Reid, G. A., and Chapman, S. K. (2001) Kinetic and crystallographic analysis of the key active site acid/base arginine in a soluble fumarate reductase. *Biochemistry 40*, 12292−12298.

(32) Doherty, M. K., Pealing, S. L., Miles, C. S., Moysey, R., Taylor, P., Walkinshaw, M. D., Reid, G. A., and Chapman, S. K. (2000) Identification of the active site acid/base catalyst in a bacterial fumarate reductase: A kinetic and crystallographic study. *Biochemistry 39*, 10695−10701.
(33) Scavetta, R. D., Herron, S. R., Hotchkiss, A. T., Kita, N., Keen, N. T., Benen, J. A., Kester, H. C., Visser, J., and Jurnak, F. (1999) Structure of a plant cell wall fragment complexed to pectate lyase C. *Plant Cell 11*, 1081−1092.
(34) Sanchez-Torres, P., Visser, J., and Benen, J. A. (2003) Identification of amino acid residues critical for catalysis and stability in *Aspergillus niger* family 1 pectin lyase A. *Biochem. J. 370*, 331−337.
(35) Guillén Schlippe, Y. V., and Hedstrom, L. (2005) Guanidine derivatives rescue the Arg418Ala mutation of *Tritrichomonas foetus* IMP dehydrogenase. *Biochemistry 44*, 16695−16700.
(36) Min, D., Josephine, H. R., Li, H., Lakner, C., MacPherson, I. S., Naylor, G. J., Swofford, D., Hedstrom, L., and Yang, W. (2008) An enzymatic atavist revealed in dual pathways for water activation. *PLoS Biol. 6*, e206.